Optical Properties of Disulfide−Functionalized Diacetylene Self-Assembled Monolayers on Gold: a Spectroscopic Ellipsometry Study

ARTICLE *in* THE JOURNAL OF PHYSICAL CHEMISTRY C · DECEMBER 2009

Impact Factor: 4.77 · DOI: 10.1021/jp906298m

Optical Properties of Disulfide-Functionalized Diacetylene Self-Assembled Monolayers on Gold: a Spectroscopic Ellipsometry Study

Mirko Prato,[†] Marina Alloisio,[‡] Sushilkumar A. Jadhav,[‡] Andrea Chincarini,[†] Tiziana Svaldo-Lanero,[||] Francesco Bisio,[§] Ornella Cavalleri,[||] and Maurizio Canepa*[,||]

Istituto Nazionale di Fisica Nucleare, Sezione di Genova, Via Dodecaneso 33, 16146 Genova, Italy, INSTM and Dipartimento di Chimica e Chimica Industriale, Università di Genova, Via Dodecaneso 31, I-16146 Genova, Italy, CNR-INFM LAMIA, Corso Perrone 24, I-16152 Genova, Italy, and CNISM and Dipartimento di Fisica, Università di Genova, Via Dodecaneso 33, 16146 Genova, Italy

Received: July 3, 2009; Revised Manuscript Received: September 21, 2009

Spectroscopic ellipsometry (SE) has been applied to study the optical properties of thiolate polydiacetylene (PDA) self-assembled monolayers (SAMs) deposited on low-roughness polycrystalline gold. A systematic investigation of methyl-terminated diacetylene (dihexacosa-7,9-diyn disulfide, DS9) SAMs is presented. The results have been compared with experiments on carbazolyl-derivatized diacetylene (14-(9*H*-9-carbazolyl)tetradeca-10,12-diyn-1-yl disulfide, CDS9) SAMs and with findings recently obtained on SAMs of alkanethiols. The SE measurements have been complemented with X-ray photoelectron spectroscopy and atomic force microscopy data. The difference between SE spectra measured after and before the monolayer assembly ($\delta\Psi = \Psi_{SAM} - \Psi_{Au}$ and $\delta\Delta = \Delta_{SAM} - \Delta_{Au}$) showed specific absorptions of the adsorbed molecules, including narrow features in the 500−700 nm wavelength range which have been interpreted as markers of the SAM polymerization state. To our knowledge, these results represent the first unambiguous optical detection of polymer-induced absorptions in the case of diacetylene SAMs. Polymerization mainly occurred in the so-called red phase (absorption peak around 550 nm) on very flat surface regions obtained by flame-annealing the sample. The polymeric phase was stable against moderate UV irradiance. The detection of the blue phase was questionable as specific absorptions (around 640 nm) overlap with an absorption band related to the formation of the S−Au interface.

I. Introduction

Since the first reports, polydiacetylenes (PDAs)[1] have been attracting continuous interest for their chromic response to stimuli of different types, such as exposure to UV light, heat, chemical agents, and mechanical stress.[2,3] The unique chromic properties of PDAs have been extensively studied in highly ordered bulk systems,[2] ultrathin films[4,5] down to self-assembled monolayers (SAM).[6,7] Optical absorptions in PDAs occur via $\pi-\pi^*$ excitation within the linear conjugated polymer backbone. The most recurrent chromic forms of PDAs are the so-called red and blue phases, with absorptions centered at about 540 and 640 nm, respectively. The blue-to-red phase transition and the absence of fluorescence response of the blue phase are most interesting for applications to sensors.[2,8,9] The chromic transition was for a long time attributed to variations of an effective conjugation length: Any twist or misalignment of the planar backbone of the fully conjugated blue phase would lead to a "less-conjugated" phase, shifting the $\pi-\pi^*$ transition to higher energy. This interpreting scheme could hardly explain the occurrence of other color forms, such as the bluish-green form,[10] and it was not able to account for the observation of long-range ordered red chains.[10,11] According to recent views, the red phase should be conceived as an electronic structure of a likely nonplanar chain and not necessarily related to disorder.[10] The color change should be therefore the output of the transition between different chain conformations.[10]

Concerning PDA SAMs an intense research stream dealt with the deposition of thiol-terminated diacetylenes on gold films exhibiting (111) texture, since an adsorption geometry similar to that of alkanethiols was expected to favor the topo-polymerization.[6,12,7] Polymerization was first demonstrated for methyl-terminated diacetylene thiols,[6] for which a blue phase was reported. 2D photopolymerization was confirmed by the studies of Crooks et al.[12] on hydroxyl- and carboxy-terminated diacetylenes. In a systematic investigation, Mowery et al. deeply examined the role of substrate morphology and the interplay between substrate−molecule and molecule−molecule interactions to obtain PDA SAMs with a high degree of conjugation.[7,13] The detection of polymerized phases in PDAs thin films has been historically carried out using optical absorption spectroscopy and Raman spectroscopy.[14] Regarding SAMs, UV−vis spectroscopy was scarcely utilized due to poor or ambiguous response[12,15] and the polymeric phase was generally identified by vibrational probes. Among optical methods, spectroscopic ellipsometry (SE) proved successful in the study of the thermochromism of an ultrathin PDA Langmuir film.[16]

In the present research, in the stream of recent achievements on thiolate interfaces,[17] we have applied SE, for the first time, to characterize the optical properties of PDA monolayers. This paper has several motivations. First, to test the SE sensitivity for the detection of excitonic absorptions in PDA SAMs. To this purpose, we have performed a systematic investigation of methyl-terminated diacetylene (dihexacosa-7,9-diyn disulfide,

* To whom correspondence should be addressed. E-mail: canepa@fisica.unige.it.
[†] Istituto Nazionale di Fisica Nucleare.
[‡] INSTM and Dipartimento di Chimica e Chimica Industriale, Università di Genova.
[§] CNR-INFM LAMIA.
[||] CNISM and Dipartimento di Fisica, Universitá di Genova.

10.1021/jp906298m CCC: $40.75
Published on Web 11/04/2009

DS9) SAMs deposited on polycrystalline gold surfaces of low roughness, a system which was already extensively studied by IR and Raman spectroscopies.[15] Second, to perform new experiments on the polymerization of carbazolyldiacetylene (14-(9*H*-9-carbazolyl)tetradeca-10,12-diyn-1-yl disulfide, CDS9) SAMs, which extend the data set presented in a preliminary report.[18] CDS9 is appealing for applications thanks to the optoelectronic properties related to the carbazolyl groups.[19] Finally, to gather new information on the interplay between the formation of the polymeric backbone and the molecule−substrate interaction, and about the influence of such interactions on the morphology of the S−Au interface,[20−22] also in relation to intriguing magnetic properties.[23,24]

II. Experimental Section

A. Methods. Standard SE measurements were performed on a rotating compensator ellipsometer (M-2000, J.A. Woollam Co. Inc.). The instrument, tested on Langmuir−Blodgett films,[25] allows simultaneous measurements at 225 different wavelengths in the range 245−725 nm. Principles of SE are described at length in several books.[26−28] In brief, the output of ellipsometry is the complex reflection coefficient ρ:

$$\rho = \frac{r_{pp}}{r_{ss}} = \tan \Psi \exp(i\Delta) \qquad (2.1)$$

where r_{pp} and r_{ss} are the Fresnel reflection coefficients for p- and s-polarization, respectively. The ellipsometer allowed to monitor the spectral evolution of Ψ and Δ in real time with a time resolution of a few seconds. Information on optical properties and thickness of thin films can be derived by comparing the experimental data with simulations based on realistic optical models of the system under investigation.[25,27,28,30] Application to SAMs requires specific methods which have been thoroughly discussed elsewhere.[17] The tiny spectral variations induced by formation of nanometer-thick layers can be appreciated by averaging, for several zones of each sample, the difference between grazing incidence spectra measured after and before the SAM formation ($\delta\Psi(\Delta) = \Psi(\Delta)_{SAM} - \Psi(\Delta)_{Au}$).[17,29,31] We will show in this paper (Section III) that SE may provide fingerprints of sharp molecular optical absorptions in SAMs through the detection of characteristic dips in high-quality difference spectra. In this work SE spectra were typically collected at 65° and 70° angle of incidence.

X-ray photoelectron spectroscopy (XPS) analysis was carried out with a PHI ESCA 5600 MultiTechnique apparatus. The system consists of an X-ray Al-monocromatised source ($h\nu$ = 1486.6 eV) and a spherical capacitor electron energy analyzer, used at a constant pass energy of 5.85 eV. In the standard configuration the analyzer axis formed an angle (takeoff angle) of 45° with the sample surface. The binding energy (BE) scale was referenced to the Au $4f_{7/2}$ level at 84.0 eV.

Tapping mode atomic force microscopy (AFM) measurements were performed using a Multimode/Nanoscope IV system (Digital Instruments) and Si cantilevers (OMCL-AC160 TS, Olympus).

B. Materials and SAM Preparation. The DS9 monomer was synthesized according to the procedure described in ref 32. Analytical and spectroscopic data were in full agreement with those reported therein. Synthesis and characterization of CDS9 monomers were described in detail elsewhere.[19]

For the SAM preparation, the substrates were incubated in 1 mM DA solution in chloroform (Sigma, purity> 98%) for 48 h at room temperature (RT). After extraction, the samples were copiously rinsed with the solvent and dried under a nitrogen stream. Sample processing was performed in the dark, in order to minimize uncontrolled photopolymerization. The SE measurements were also performed in the dark, initially filtering the Xe lamp UV radiation. Upon filter removal, real-time SE measurements were performed to monitor any variation induced by the lamp's own radiation. Samples were then typically irradiated for 20 min using a Mineralight UVG-11 lamp placed 2 cm apart.

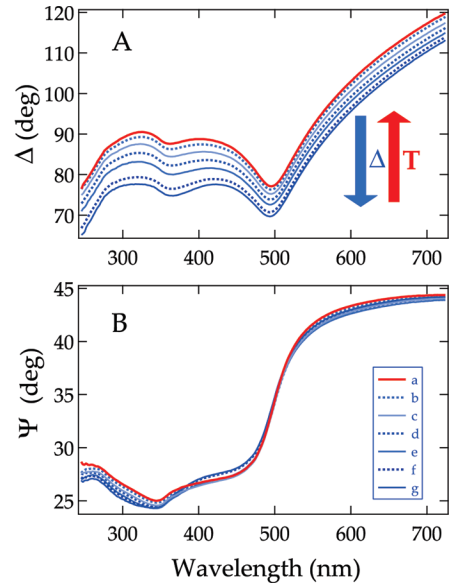

Figure 1. SE spectra (70° angle of incidence) of representative Au substrates used in the experiment. Curves a (red) are representative of "softly" annealed substrates, for which Cr segregation was ignorable. Corresponding dielectric constants (cf. ref 17) were in good agreement with benchmark literature.[34] Curves b−g illustrate the effect of the annealing duration. Longer annealing durations induced larger Δ downward shifts. The rigid Δ shifts in the 550−725 nm range have been utilized to classify the substrates along the series as explained in the text.

Regarding Au substrates, we chose the commercial samples (Arrandee) successfully adopted in recent works on alkanethiolate SAMs.[17,31,33] These substrates consist of a nominally 200-nm-thick Au film evaporated on glass slides coated with a Cr primer. They were preferred to gold/mica samples because of their highly homegeneous optical response over the macroscopic scale of the light spot on the sample (a few mm^2), preserved after the annealing. This property ensured the minimization of the uncertainty involved in the calculation of SE difference spectra from ex-situ measurements made before and after incubation in solution. In a first series of measurements we replicated the substrate preparation procedure of recent works.[17,33] The key aspect of this procedure was a "soft" flame annealing that proved effective to reduce the surface roughness and the amount of adventitious contaminants without inducing significant surface segregation of Cr atoms. In a second series, the annealing duration was progressively prolonged with the aim of reducing the surface roughness to a greater extent. Under the flame, the temperature was empirically judged by looking at the sample chromic gradation. Soon after the treatment and before incubation, SE measurements provided a more quantitative criterion for the classification of substrates. In Figure 1, curves a (red) represent SE spectra obtained for soft annealing. Curves b−g illustrate the effects of prolonged annealing. The pseudodielectric constants derived from spectra of Figure 1 (not

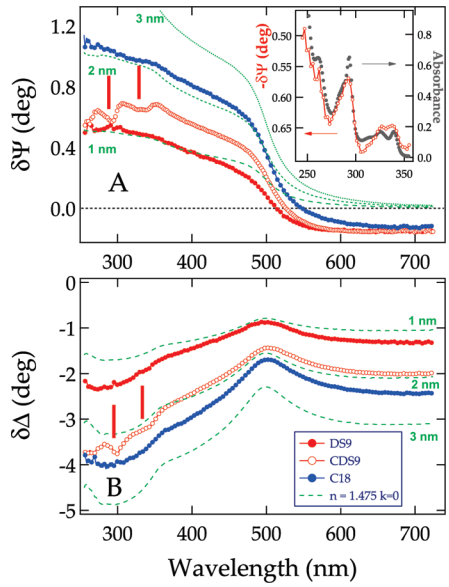

Figure 2. $\delta\Psi$ and $\delta\Delta$ difference spectra (70° angle of incidence) for DS9 and CDS9 SAMs deposited on softly annealed substrates (cf. curves a of Figure 1). Measurements on alkanethiols C18 SAMs are reported for comparison. Dashed lines (green) are simulations of a three-phases model (ambient/film/substrate) for transparent films (index of refraction $n = 1.475$) of different thickness. Thin bars at about 295 and 330 nm emphasize narrow features in the CDS9 SAM spectra. As highlighted in the inset, where the CDS9 $-\delta\Psi$ pattern (red markers) is compared with the UV−vis absorption spectrum measured on a 1 mM CDS9 solution (dark gray markers), these features are related to absorptions of the carbazolyl ring.

shown) significantly deviated from benchmarks[34,17] and presented relatively strong extra-absorptions below 400 nm. As also suggested by XPS and AFM experiments (see later on the paper), curves b−g likely reflect complex changes of both chemical and morphologic character. XPS data in particular showed surface oxide species formed after the migration of Cr atoms from the adhesive layer. A detailed simulation of all the experimental curves went far beyond the scope of this paper.

Nevertheless, it was necessary to find out a parameter able to represent, to a reasonable degree of approximation, the annealing temperature or, at least, the annealing stage. To this purpose we focused the attention on the rigid spectral shifts observed in the 550−725 nm spectral range of Δ spectra (panel A). In this spectral region, the average absolute value of the Δ shift of a given annealed substrate with respect to curve a of Figure 1 turned out, to a good approximation, to be proportional to the annealing time. For practical purposes, in the remaining part of the paper, we will denote this parameter as $\delta\Delta^{T}_{sub}$.

III. Results

Figure 2 shows representative ex-situ $\delta\Psi$ and $\delta\Delta$ patterns obtained on DS9 and CDS9 SAMs deposited on softly annealed substrates.

Data are compared with measurements on C18 alkanethiol SAMs, about 2.3 nm thick,[17] deposited on the same type of substrates. Simulations are also shown for transparent layers with thickness in the 1−3 nm range and 1.475 index of refraction, a reasonable approximation for packed alkyl chains.[17] These simulations provide a useful graphical frame of reference for an empirical estimate of the layer thickness. Note that for ultrathin transparent films of given refraction index $\delta\Delta$ patterns are proportional to the thickness. $\delta\Psi$ curves exhibited a well-defined transition from positive to negative values at about 500

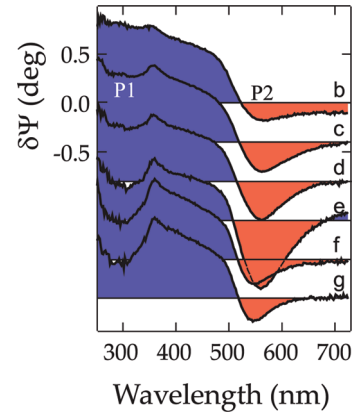

Figure 3. $\delta\Psi$ difference spectra obtained for DS9 SAMs deposited on substrates b−g of Figure 1. Each difference spectrum was calculated with reference to the spectrum measured on its pertinent substrate after annealing and before incubation, thus bringing direct information on the molecular-induced spectral changes. The curves are offset for the sake of clarity.

nm, in correspondence to the $\delta\Delta$ maximum, and then approached a common value of about −0.14° in the NIR limit. While reproducing some gross features of experimental patterns, a transparent layer model (e.g., dashed curves) could not account for negative NIR $\delta\Psi$ values, which were assigned to absorptions located at the S−Au interface[17] and for the narrow features that were observed in the CDS9 patterns at about 295 and 330 nm, highlighted by thin bars in the figure. The $\delta\Psi$ features can be directly assigned to molecular absorptions through a comparison with optical transmission measurements performed on a 1 mM CDS9 solution. This comparison is highlighted in the inset of panel A. Zooming in the 245−350 nm range, the $-\delta\Psi$ sharp features nicely matched the UV−vis absorption peaks related to the carbazolyl group. For deposition on "softly" annealed substrates, we could not discriminate any peaked features in the region of interest of the polymer excitons, around 540 and/or 640 nm, even after postgrowth UV irradiance. This finding is fully consistent with the empirical film thickness that can be valuated from Figure 2. In this respect we note that the larger thickness of the CDS9 SAM compared to the DS9 layer would be fully consistent with the molecules structure; however, the ellipsometric thickness has to be related to both the molecular size and the packing density. Anyway, values of the ellipsometric thickness in the 1−2 nm range suggested that the diacetylenes SAMs of Figure 2 present a high degree of disorder with a large fraction of tilted molecules. New, relatively sharp features in the spectral region of interest for polymer absorptions were instead observed in a second series of experiments, dealing with DS9 deposition on heavily annealed substrates. $\delta\Psi$ spectra obtained after the SAM deposition on the substrates b−g of Figure 1 are shown in Figure 3. Corresponding $\delta\Delta$ spectra are reported in the Supporting Information. Concentrating on $\delta\Psi$ spectra, well-defined dips were observed in the 260−350 nm region (P_1) and in the 500−600 nm region (P_2). In both spectral regions, the DS9 monomer does not exhibit specific absorptions. P_2 was peaked at about 555 nm in curve e, where it showed a broad tail extending toward the NIR region. In curves f−g the feature shifted at about 545 nm and the low-energy tail appeared severely reduced. Unlike P_2, P_1 was also observed, though with a reduced magnitude, in control experiments on C18 films deposited on heavily annealed substrates (cf. Supporting Information).

Figure 3 suggested a different evolution of P_1 and P_2 intensity along the measurement series. Later on the paper P_1 and P_2

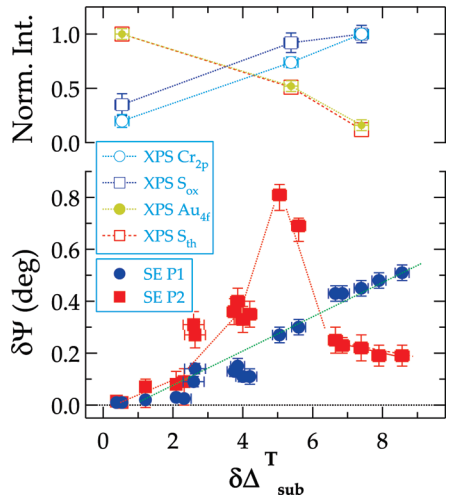

Figure 4. Lower panel: Intensity of the SE P_1 and P_2 features (cf. Figure 3) as a function of $\delta\Delta^T_{sub}$. Note that the data points considered an ensemble of measurements more extended than the one of Figure 3. Upper panel: Intensity of selected XPS peaks obtained from measurements on samples b−f of Figure 3. The Au 4f and the S_{th} peaks (cf. Figure 6) have been normalized to the data of sample b while the Cr 2p and the S_{ox} peaks (cf. Figure 6) have been normalized to the data of sample f. Lines are guide for eyes.

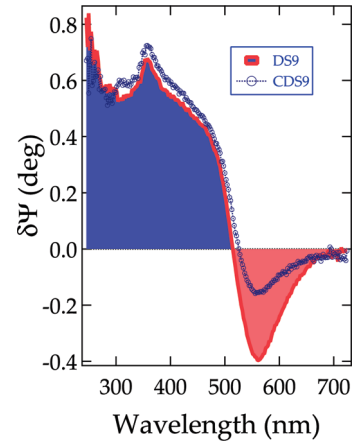

Figure 5. Comparison between $\delta\Psi$ difference spectra obtained for DS9 and CDS9 SAMs deposited on heavily annealed substrates of comparable quality. Note that for CDS9 the P_1 features are somewhat mixed with the small peaks related to the carbazolyl group absorptions (cf. Figure 2).

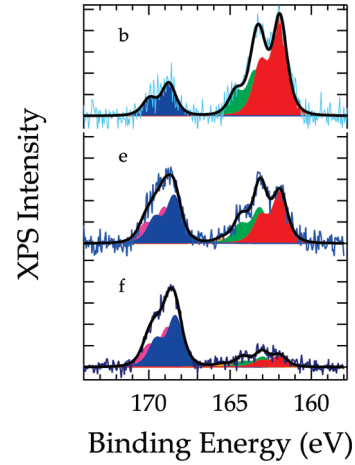

Figure 6. XPS measurements dedicated to the S 2p core level BE region on samples b−f of Figure 3. For details on fitting and peak labeling see text.

will be assigned to different adsorption configurations. It proved useful to plot the P_1 and P_2 intensity as a function of the $\delta\Delta^T_{sub}$ parameter. That is shown in the lower panel of Figure 4. A fair definition of the P_1 and P_2 area was ambiguous. For the P_1 intensity, we considered the absolute difference between the evident maximum at about 360 nm and the bottom of the feature, at about 300 nm. For P_2, we simply took the absolute difference between the peak and the NIR data. Though these criteria present some degrees of arbitrariness, inspection of Figure 3 instills confidence that the reported patterns catched the essential trends. P_1, approximately constant for low $\delta\Delta^T_{sub}$ values, showed a roughly linear increase. P_2 exhibited a neat maximum followed by a sharp drop and a moderate decrease for high $\delta\Delta^T_{sub}$ values. Less systematic measurements were also performed for CDS9 SAMs. A comparison between data of CDS9 and DS9 SAMs obtained on softly annealed substrates has been shown in Figure 2. Heavy annealing of substrates was again necessary to observe well-defined P_2 features, generally less pronounced than in the DS9 case. Strong P_1 dips were observed as well. A comparison between CDS9 and DS9 data obtained on heavily annealed substrates of comparable quality (i.e., with a closely similar $\delta\Delta^T_{sub}$) is reported in Figure 5. Note that, despite the different intensity, the P_2 feature exhibits the same position and similar shape in both spectra.

Focusing back on DS9 data, in order to add information on chemical and morphologic changes occurring after prolonged annealing, ancillary XPS and AFM measurements were also performed, focusing on samples b−f of Figure 3. Regarding the Au 4f and the Cr 2p peaks, the main outputs of the measurements (reported in the Supporting Information) are summarized in the upper panel of Figure 4. The increase of $\delta\Delta^T_{sub}$ was accompanied by a net increase of the Cr 2p intensity and a drop of Au levels intensity. The position of the Cr 2p core level (3/2 component at about 576.6 eV BE) suggested the occurrence of Cr_2O_3 species. Representative high-resolution XPS measurements dedicated to the S 2p region are shown in Figure 6. The fitting procedure adopted was described in details elsewhere.[35,36] For each S 2p doublet, a 1.2 eV energy splitting and a 2:1 intensity ratio between the 3/2 and 1/2 components were applied.[35,36] The same width was assumed for all peaks. The states were identified in terms of the position of the 3/2 peak. In all patterns, two states were disentangled, at 162 (S_{th}) and 163.4 eV (S_{dis}) BE. These states appeared appreciably attenuated in curve e and f where the best fit required a third, very small doublet at about 164.3 eV. S_{th} matched the strong attenuation of the Au signal, as reported in Figure 4, and it was assigned to the S−Au bond formation.[35−38] S_{dis} was assigned to the disulfide bond of unreacted molecules.[39] Another doublet, S_{ox}, observed at about 168.8 eV in curve b, evolved in an intense and broadened feature in spectra e and f, where two doublets, at 168.5 and 169 eV, were necessary to obtain the best fit. The energy position of S_{ox} was fairly consistent with oxidized sulfur species.[40] Indeed, as reported in Figure 4, the intensity of S_{ox} approximately scaled with the intensity of the Cr signal.

Concerning the AFM measurements, the increase of $\delta\Delta^T_{sub}$ induced an overall increase of the rms roughness, R_{av}, that was measured on relatively large scale (10 μm × 10 μm) images. A representative image obtained on sample e of Figure 3 is reported in Figure 7. Corresponding data on samples b and f have been reported in the Supporting Information. R_{av} changed from about 3 nm, on softly annealed samples, up to more than 5 nm on sample f. On sample e many large (typically a few μm^2), and flat zones, characterized by a small local roughness

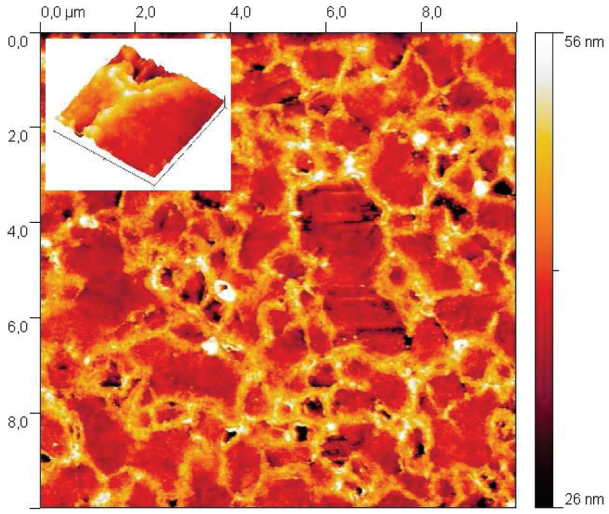

Figure 7. AFM image (10 μm × 10 μm) obtained on sample e of Figure 3. The inset (3D zoom on a 1 μm × 1 μm area) emphasizes the presence of outcrops at the borders of flat grains.

($R_{loc} \simeq 1$ nm) were observed. The value of R_{av} was affected by protrusions, a few tens of nm high, well visible at the borders of flat zones. On the heaviest annealed substrates, such as sample f and g of Figure 3, the protrusions increased in statistical importance and only a relatively few, small scale, very flat zones ($R_{loc} \leq 1$ nm), could still be found. We interpreted such protrusions as due to Cr outcrops, initially localized at grain borders, then spreading on the whole surface for higher and higher $\delta\Delta^T_{sub}$.

IV. Discussion

Cross-comparison of the SE and the XPS outcomes, summarized in Figure 4, led to assign P_1 and P_2 to different molecular adsorption states.

The intensity of P_1 increased along with the surface amount of Cr and with S_{ox}. It was consequently assigned to the bond of DS9 molecules with Cr oxide species. The bond likely involved the dissociation of the disulfide bridge with formation of oxidized sulfur species.[41] On the other hand the behavior of P_2, particularly the intensity drop on heavily annealed substrates, strongly supported an assignment to molecules adsorbed at gold sites. For the largest $\delta\Delta^T_{sub}$ values, the position of P_2 matched the characteristic wavelength of the red-phase observed in many bulky systems. On samples b−e, the position was slightly red-shifted, yet still compatible with an assignment to red-phase chains.[16,42] Note that in their SE study about ultrathin Langmuir PDA films Carpick et al. disentangled one main peak at about 551 nm and a broader satellite line at 506 nm.[16] The latter was difficult to disentangle in our experiment due to the $\delta\Psi$ positive-to-negative transition, common to any thiolate SAMs.

Early works on SAMs did not provide sharp optical evidence of polymerization. Transmission measurements on SAMs-covered Au ultrathin films reported on an absorbance band monotonously increasing in the 500−800 nm wavelength region. The evolution of the band into a broad peak at about 620 nm after UV irradiation was assigned to photoinduced polymerization.[12,43] However, an ensuing work claimed a similar behavior on SAMs of alkanethiols, concluding with a note of general skepticism about the possibility of direct detecting SAMs polymerization by UV/vis spectroscopy.[15]

In our work, the cross-comparison between SE and AFM suggested that polymerization preferentially occurred on locally flat regions (rms roughness ≤1 nm) in agreement with the discussion of ref 13. However, we did not get evidence of the blue form and we did not observe significant effects of moderate postincubation UV irradiance. These finding agree with SERS data of some of us about DS9 and CDS9 SAMs polymerization on rough gold platforms[19] but appear at variance with early works, where Raman measurements indicated a significant blue form population. Indeed, we cannot exclude that broadened features, possibly related to short blue- or even purple-phase chains could be hidden in the negative $\delta\Psi$ background of spectra of Figure 2,[18] as well as in the evident tail extending toward the low energy side of $\delta\Psi$ c−e patterns of Figure 3. Considering that early works were conducted on films directly deposited on mica slides,[7] we must mention the possibility that some Cr segregation occurring within flat zones and not only at grain borders could have affected the polymerization process destabilizing the blue phase. Anyway, the discrepancy of our results with previous reports[6,7] is not completely surprising in view of the well-known delicate interplay between polymerization and substrate quality and deposition conditions.[7] There are growing indications that constraints from the side groups may play a definite role in governing the PDA color.[10] In the case of molecules strongly bound to the surface, the surface itself should be conceived as a sort of extended "side group". Viewed from this perspective, the formation of the blue-phase for a thiolate DA SAMs appears as a rather critical process, involving the simultaneous formation of S−Au bonds and of the polymer backbone, i.e., the formation of a very "rigid" planar structure. The process appears even more critical in the case of CDS9 molecules where the steric hindrance of the carbazole termination comes into play. It is therefore conceivable that our preparation conditions could have favored the lowest free-energy twisted geometry.

Related to these aspects, we draw the attention on a final point. In curves c−e the progressive growth of P_2 was accompanied by an evident decrease of the quasi-constant, negative $\delta\Psi$ signal above 500 nm, still appreciable on curve b of Figure 3. This spectral feature was tentatively assigned to a Drude-like absorption band,[17] possibly related to the interface roughening consequent to the formation of the S−Au bond. The increasing weight of Cr oxide patches explains only partly its annealing-induced attenuation. In facts XPS of sample e still showed a small yet significant S_{th} intensity. The origin of the thiol-induced interface roughening is a matter of current debate.[21,22] Under the perspective of the model of ref 21, the formation of the PDA SAMs, even in most flexible red-phase architecture, is expected to strongly engage adatoms thus reducing the dynamic interface roughening and possibly explaining the NIR $\delta\Psi$ behavior of this work.

V. Concluding Remarks

We have applied SE to characterize thiolate PDA SAMs deposited on low-roughness polycrystalline gold surfaces obtained by flame annealing. We have systematically investigated methyl-terminated (dihexacosa-7,9-diyn disulfide, DS9) SAMs. The results have been compared with experiments on carbazolyldiacetylene (14-(9*H*-9-carbazolyl)tetradeca-10,12-diyn-1-yl disulfide, CDS9) SAMs and with recent results on SAMs of simple alkanethiols deposited on substrates of comparable quality. The SE data have been complemented with XPS and AFM measurements. We have shown that through the detection of characteristic dips in high-quality difference spectra, measured after and before formation of the SAM, SE may provide direct information on specific UV−vis absorptions of the adsorbed

molecules. In particular, our data indicate that SE has the sensitivity required to allow the direct (i.e., optical) characterization of the color of PDA SAMs, through the observation of narrow absorptions in the 500−700 nm wavelength range. Cross-comparison between SE and AFM measurements indicated that polymerization mainly occurred in the so-called red phase, with a main absorption peak around 550 nm, on very flat zones of the samples (local roughness ≤1 nm). These results, to our knowledge, represent the first unambiguous optical detection of polymer-induced absorptions on PDA SAMs. The polymeric phase was stable against moderate UV irradiance. The detection of the blue phase was questionable as specific absorptions overlap with an absorption band related to the formation of the S−Au interface.

In order to improve the quality of the polymerized phase and eventually obtain the formation of the blue-form, possible developments of this work require improved substrates and involve new experimental approaches. Gold/mica substrates endowed with the macroscopic optical quality required to obtain reliable SE difference spectra seem the best candidate to overcome annealing-induced segregation problems. Incubation at temperature significantly higher than RT could be attempted to favor SAM organization and polymerization. In-situ SE measurements could be performed to monitor the evolution of the polymerization form during incubation. These kinds of measurements involve the substitution of chloroform with another suitably effective organic solvent. The achievement of dense, highly ordered polymerized phases on better defined substrates could boost the attempt to build up simulations of the SAM optical properties, which need a realistic description of the excitonic absorptions. Such a model is a prerequisite to confront the question of the determination of the polymerized fraction. In this respect and for a closer comparison with early literature on PDA SAMs, it would be worth combining SE and surface Raman experiments on samples prepared under the same experimental conditions.

Acknowledgment. This research has been supported by the University of Genova, MIUR (PRIN 2006020543003) and Fondazione Carige. The authors thank the organic chemistry group of the University of Genova for providing DS9 and CDS9 molecules and acknowledge the experimental support of L. Lavagnino and P. Renati in first stages of the work. Further the authors thank C. Cuniberti, G. Dellepiane, and A. Gliozzi for their continuos support to the project. F.B. acknowledges the CNR-CNISM convention for financial support. The authors thank V. Esaulov, H. Hamoudi, and A. Cossaro for discussions.

Supporting Information Available: Additional spectra and AFM images. This material is available free of charge via the Internet at http://pubs.acs.org.

References and Notes

(1) Tieke, B.; Lieser, G.; Wegner, G. *J. Polym. Sci. Polym. Chem.* **1979**, *17*, 1631.

(2) *Polydiacetylenes*; Cantow H. J., Ed.; Springer: Berlin, 1984; *Polydiacetylenes*; Bloor D., Chance R. R., Eds.; Martinus Nijhoff: Dordrecht, 1985.

(3) Charych, D. H.; Nagy, J. O.; Spevak, W.; Bednarski, M. D. *Science* **1993**, *261*, 585.

(4) Carpick, R. W.; Sasaki, D. Y.; Marcus, M. S.; Eriksson, M. A.; Burns, A. R. *J. Phys.: Condens. Matter* **2004**, *16*, R679R697.

(5) Sasaki, D. Y.; Carpick, R. W.; Burns, A. R. *J. Colloid Interface Sci.* **2000**, *229*, 490.

(6) Batchelder, D. N.; Evans, S. D.; Freeman, T. L.; Hiussling, L.; Ringsdorf, H.; Wolf, H. *J. Am. Chem. Soc.* **1994**, *116*, 1050.

(7) Menzel, H.; Mowery, M. D.; Cai, M.; Evans, C. E. *Macromolecules* **1999**, *32*, 4343.

(8) Leclerc, M. *Adv. Mater.* **1999**, *11*, 14911498.

(9) Dong, June Ahn; Jong-Man, Kim *Acc. Chem. Res.* **2008**, *41*, 805.

(10) Schott, M. *J. Phys. Chem. B* **2006**, *110*, 15864.

(11) Barisien, T.; Legrand, L.; Weiser, G.; Deschamps, J.; Balog, M.; Boury, B.; Dutremez, S. G.; Schott, M. *Chem. Phys. Lett.* **2007**, *444*, 309.

(12) Kim, T.; Ye, Q.; Sun, L.; Chan, K. C.; Crooks, R. M. *Langmuir* **1996**, *12*, 6065.

(13) Mowery, M. D.; Menzel, H.; Cai, M.; Evans, C. E. *Langmuir* **1998**, *14*, 5594.

(14) (a) Koshihara, S.; Tokura, Y.; Takeda, K.; Koda, T. *Phys. Rev. Lett.* **1992**, *68*, 1148. (b) Deckert, A. A.; Fallon, L.; Kiernan, L.; Cashin, C.; Perrone, A.; Encalarde, T. *Langmuir* **1994**, *10*, 1948. (c) Huggins, K. E.; Son, S.; Stupp, S. I. *Macromolecules* **1997**, *30*, 5305.

(15) Menzel, H.; Mowery, M. D.; Cai, M.; Evans, C. E. *J. Phys. Chem. B* **1998**, *102*, 9550.

(16) Carpick, R. W.; Mayer, T. M.; Sasaki, D. Y.; Burns, A. R. *Langmuir* **2000**, *16*, 4639.

(17) Prato, M.; Moroni, R.; Bisio, F.; Rolandi, R.; Mattera, L.; Cavalleri, O.; Canepa, M. *J. Phys. Chem. C* **2008**, *112*, 3899.

(18) Cavalleri, O.; Prato, M.; Chincarini, A.; Rolandi, R.; Canepa, M.; Gliozzi, A.; Alloisio, M.; Lavagnino, L.; Cuniberti, C.; DellErba, C.; Dellepiane, G. *Appl. Surf. Sci.* **2005**, *246*, 403408.

(19) Alloisio, M.; Demartini, A.; Cuniberti, C.; Petrillo, G.; Thea, S.; Giorgetti, E.; Giusti, A.; Dellepiane, G. *J. Phys. Chem. C* **2007**, *111*, 345.

(20) Maksymovych, P.; Sorescu, D. C.; Yates, J. T., Jr. *Phys. Rev. Lett.* **2006**, *97*, 146103.

(21) Mazzarello, R.; Cossaro, A.; Verdini, A.; Rousseau, R.; Casalis, L.; Danisman, M. F.; Floreano, L.; Scandolo, S.; Morgante, A.; Scoles, G. *Phys. Rev. Lett.* **2007**, *98*, 016102.

(22) Yu, M.; Bovet, N.; Satterley, C. J.; Bengio, S.; Lovelock, K. R. J.; Milligan, P. K.; Jones, R. G.; Woodruff, D. P.; Dhanak, V. *Phys. Rev. Lett.* **2006**, *97*, 166102.

(23) (a) Neuman, O.; Naaman, R. *J. Phys. Chem. B* **2006**, *110*, 5163. (b) Carmeli, I.; Leitus, G.; Naaman, R.; Reich, S.; Vager, Z. *J. Chem. Phys.* **2003**, *118*, 10372.

(24) Suda, M.; Kameyama, N.; Ikegami, A.; Einaga, Y. *J. Am. Chem. Soc.* **2009**, *131*, 865.

(25) Gonella, G.; Cavalleri, O.; Emilianov, I.; Mattera, L.; Canepa, M.; Rolandi, R. *Mater. Sci. Eng., C* **2002**, *22*, 359.

(26) Azzam, R. M. A.; Bashara, N. M. *Ellipsometry and Polarized Light*; North Holland: Amsterdam, 1987.

(27) *Handbook of Ellipsometry*; Tompkins, H. G., Irene E. A., Eds.; William Andrew, Inc., Springer: New York, 2005.

(28) Fujiwara; H. *Spectroscopic Ellipsometry: Principles and Applications*; Wiley and Sons: New York, 2007.

(29) Shi, J.; Hong, B.; Parikh, A. N.; Collins, R. W.; Allara, D. L. *Chem. Phys. Lett.* **1995**, *246*, 90.

(30) Woollam, J. A.; Johs, B.; Herzinger, C. M.; Hilfiker, J. N.; Synowicki, R.; Bungay, C. *SPIE Proc.* **1999**, *CR72*, 1.

(31) Bordi, F.; Prato, M.; Cavalleri, O.; Cametti, C.; Canepa, M.; Gliozzi, A. *J. Phys. Chem. B* **2004**, *108*, 20263.

(32) Mowery, M. D.; Evans, C. E. *Tetrahedron Lett.* **1997**, *38*, 11.

(33) Hamoudi, H.; Guo, Z.; Prato, M.; Dablemont, C.; Zheng, W. Q.; Bourguignon, B.; Canepa, M.; Esaulov, V. A. *Phys. Chem. Chem. Phys.* **2008**, *10*, 6836.

(34) Aspnes, D. E.; Kinsbron, E.; Bacon, D. D. *Phys. Rev. B* **1980**, *21*, 3290.

(35) Gonella, G.; Terreni, S.; Cvetko, D.; Cossaro, A.; Mattera, L.; Cavalleri, O.; Rolandi, R.; Morgante, A.; Floreano, L.; Canepa, M. *J. Phys. Chem. B* **2005**, *109*, 18003.

(36) Cavalleri, O.; Gonella, G.; Terreni, S.; Vignolo, M.; Pelori, P.; Floreano, L.; Morgante, A.; Canepa, M.; Rolandi, R. *J. Phys.: Condens. Matter* **2004**, *16*, S2477.

(37) Castner, D. G.; Hinds, K.; Grainger, D. W. *Langmuir* **1996**, *12*, 5083.

(38) Duwez, A. *J. Electron Spectrosc. Relat. Phenom.* **2004**, *134*, 97138.

(39) Heister, K.; Zharnikov, M.; Grunze, M; Johansson, L. S. O.; Ulman, A. *Langmuir* **2001**, *17*, 8.

(40) Hoertz, P. G.; Niskala, J. R.; Dai, P.; Black, H. T.; You, W. *J. Am. Chem. Soc.* **2008**, *130*, 9763.

(41) Petrovykh, D. Y.; Kimura-Suda, H.; Opdahl, A.; Richter, L. J.; Tarlov, M. J.; Whitman, L. J. *Langmuir* **2006**, *22*, 2578.

(42) Cavallo, D.; Alloisio, M.; DellErba, C.; Cuniberti, C.; Comoretto, D.; Dellepiane, G. *Synth. Met.* **2002**, *127*, 71.

(43) Kim, T.; Crooks, R. M.; Tsen, J. M.; Sun, L. *J. Am. Chem. Soc.* **1995**, *117*, 3963.

JP906298M